PRAMANA
— journal of
physics

Vol. 75, No. 6
December 2010
pp. 1259–1266

Solidification and microstructural aspects of laser-deposited Ni–Mo–Cr–Si alloy on stainless steel

REENA AWASTHI*, SANTOSH KUMAR, D SRIVASTAVA and G K DEY
Materials Science Division, Bhabha Atomic Research Centre, Mumbai 400 085, India
*Corresponding author. E-mail: reena@barc.gov.in

Abstract. Laser cladding of stainless steel substrate was carried out using Ni–32Mo–15Cr–3Si (wt%) alloy powder. Laser cladding parameters were optimized to obtain defect-free and metallurgically bonded clad. Variation in solidification rate, cooling rate and compositional variation resulted in heterogeneous microstructure. Microstructure was found to be distinctly different in regions of clad cross-section. Majority of the region was found to consist of eutectic of Mo-rich hcp intermetallic Laves phase and NiFe fcc gamma solid solution phases. Extensive microstructural examinations of different clad regions have been carried out using microscopy and microanalysis techniques.

Keywords. Laser cladding; microstructure; Ni–Mo–Cr–Si alloy.

PACS Nos 42.62.-b; 81.65.-b; 81.16.Mk; 81.15.-z

1. Introduction

Hardfacing is commonly employed to produce coatings that protect the underlying substrate against wear, abrasion and corrosion and to improve the service life of the components. Traditionally, welding and thermal spraying are the most commonly employed hardfacing techniques. Laser cladding is one of the surface modification techniques, which utilizes the high-power density available from focussed laser sources and it provides uniform, homogeneous and dense coating that is metallurgically bonded to the substrate with minimal dilution and low distortion [1–3]. Large temperature gradient across the interface of the melted region and the underlying solid substrate results in rapid solidification which can give rise to extended solid solubility of the alloying elements, formation of noble metastable phases and development of a fine sub-structure in the clad that has superior physical, chemical and mechanical properties. Hardfacing of austenitic stainless steels is generally carried out to improve their hardness and wear resistance [4]. Cobalt- and nickel-based tribaloy alloys, having M–Mo–Cr–Si(M–Co,Ni) composition, have been described as alloys resistant to both corrosion and wear over a wide range of temperatures and environments [5]. Hardfacing alloys containing cobalt and boron

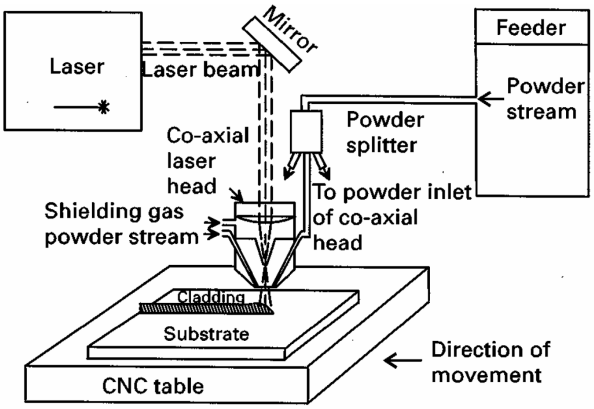

Figure 1. Schematic diagram of the laser cladding process.

are not suitable for nuclear applications, and therefore, in the present work nickel-based alloy powder, namely, Ni–32w%Mo–15w%Cr–3w%Si (equivalent to Tribaloy 700), has been used for nuclear applications. Microstructural characterization is important for controlling the quality of the laser cladding as well as to understand the metallurgical interaction between the substrate and the clad. In the present study optical microscopy, scanning electron microscopy and transmission electron microscopy (TEM) with energy dispersive spectrometer were used to study the microstructure of the clad and its constituents.

2. Experimental procedure

CO_2 laser was used to create a melt pool and, simultaneously, a jet of metal powder was directed into the melt pool using a Metco powder feeder. Laser power of 4–5 kW, substrate speed of 400–650 mm/min and powder feed rate of 9–14 g/min were used in the present study for laser cladding of stainless steel-316 L substrate. The spot size of the defocussed laser beam at the substrate surface was $\approx$5 mm for all the samples. The laser cladding head was oscillated to obtain 1–2 mm thick, 12 mm wide cladding layer with 60% overlapping for multipass cladding for area coverage. The hardness of the clad layers across the substrate–clad interface was determined by a Vickers microhardness tester using 100 g load. Cross-sectional specimens for examination by optical microscopy and SEM were polished and etched by a solution of HNO_3, HCl and glycerol in a ratio of 1:3:2 by volume. Thin foils for TEM were prepared by a jet polisher using a mixture of perchloric acid and methanol in a ratio of 1 : 4 by volume as the electrolyte at 20 V. Microstructural and compositional analysis of the sample were carried out in a JEOL-2000 FX and Tecnai microscopes. SEM was carried out in a CAM-SCAN microscope.

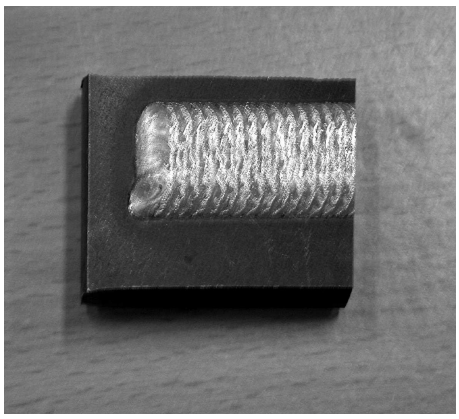

Figure 2. The geometry of the as-deposited clad.

3. Results and discussion

3.1 *Laser cladding process parameter optimization*

The schematic of the laser cladding process is shown in figure 1. Laser power of 4–5 kW, translation speed of 400–650 mm/min and powder feed rate of 9–14 g/min were optimized to achieve defect-free clad bead. The laser clad samples processed at different parameters are listed in table 1. Visually, the clad appeared continuous without lack of adherence. The as-deposited laser clad sample is shown in figure 2. The cross-sectional profile of a single clad pass which is a general reference for actual cladding application were measured in terms of width to height ratio (w/h) and listed in table 1. It was observed that the w/h ratio of the single-clad passes decreases with increasing powder feed rate (PFR) and increases with increasing translation speed (TS) at constant power because PFR increases the powder flow per unit cladding length increases and w/h ratio decreases. On the other hand, with the increase in TS, less powder available per unit length of the clad pass leads to increase in w/h ratio. It was observed that the hardness of the clad is more at higher PFR and lower TS which may be attributed to the increase in percentage of the hard phases in the microstructure. It was also observed that the samples cladded at higher power input (5 kW) exhibit significantly lower hardness than that cladded at lower power input (4 kW).

3.2 *Microstructure characterization*

The microstructure of the laser clad sample with 5 kW laser power, 14 g/min PFR, 430 mm/min TS, which produced the lowest hardness, was extensively studied by optical microscopy, scanning electron microscope and transmission electron microscopy. The cross-section of the clad revealed the appearance of uniform clad layer without lack of adherence with the substrate and defects such as crack and

Table 1. Laser clad samples at various parameters.

Sample	Power (kW)	Scanning speed (mm/min)	Feed rate (g/min)	Clad geometry (w/h)	Hardness (HVN)
1	4	435	14	6.67	760–580
2	4	650	14	9.37	650–550
3	4	435	9.3	8.10	500–440
4	4	650	9.3	13.33	580–500
5	5	435	14	6	450–400
6	5	650	14	8.82	550–500
7	5	870	14	12.5	470–440
8	5	650	9.3	15	450–410

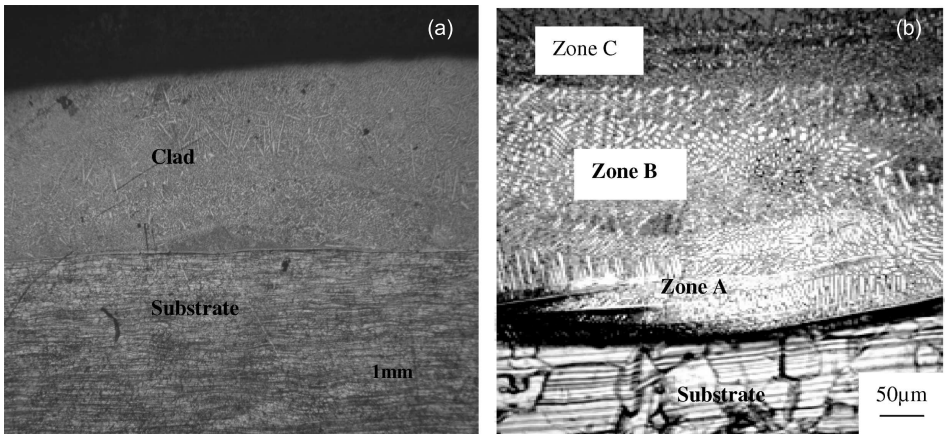

Figure 3. (**a**) Cross-sectional view of a laser clad layer (process parameters: Power = 5 kW, speed = 435 mm/min, feed rate = 14 g/min), (**b**) optical micrograph showing different regions in the cross-section of the clad layer.

porosity (figure 3a). The optical micrograph showed different solidified zones and solidification morphology, i.e. planar, cellular and dendrite microstructure in the clad layer (figure 3b).

The SEM micrographs of different solidification regions, i.e. interfacial region, (zone A), clad central region (zone B) and near-surface region (zone C) are shown in figure 4. It clearly revealed two distinct contrasts of bright and gray phases with various morphologies in clad cross-section. The microstructure of zone A extending up to 100 μm features relatively coarser columnar dendrites and interdendritic eutectic constituents near the substrate/clad interface. In zone B cellular-type microstructure with rounded morphology were observed. Zone C (extending beyond 250 μm up to the surface of the clad) microstructure had a different eutectic structure in which the brighter and darker constituents form eutectic colonies consisting of fine lamellar eutectic phase (spacing $\sim$0.1–0.2 μm). Thus majority of the region was found to consist of lamellar eutectic of bright and dark contrast phases. The

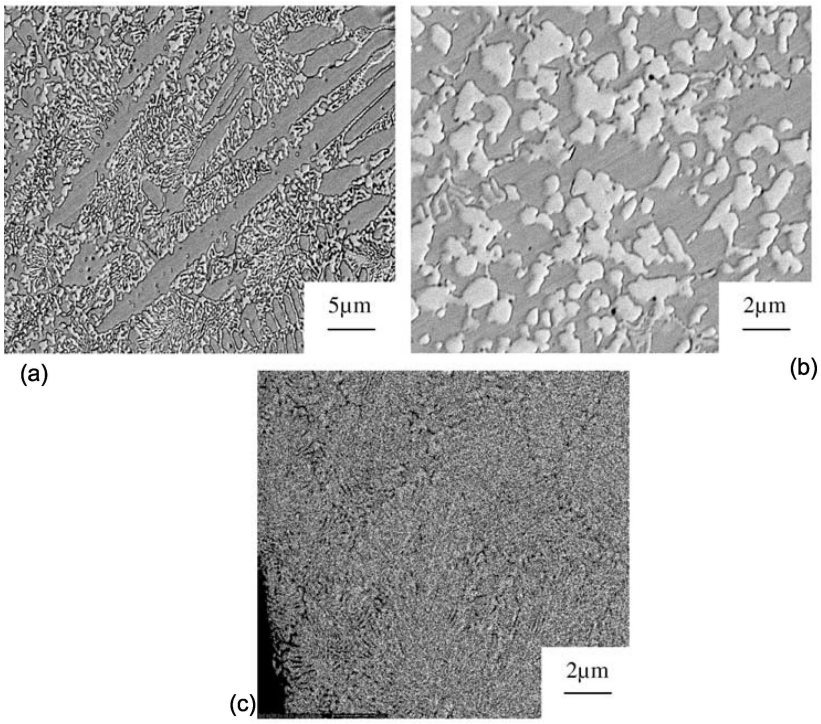

Figure 4. SEM micrograph showing (**a**) interfacial zone A showing columnar dendrites and interdendritic eutectic, (**b**) track centre zone B, (**c**) near-surface zone C showing eutectic colonies consisting of lamellar eutectic phases (bright and dark contrast).

bright and dark fields TEM images and SAD pattern of the two phases present in lamellar eutectic structure are shown in figure 5 (opposite contrast than SEM). The SAD pattern from one of the eutectic phases possesses hexagonal closed-packed intermetallic laves phase dispersed in fcc base gamma solid solution phase. The compositional analyses at various regions of clad cross-section were carried out by EDS technique attached to SEM and TEM. Mo and Si were found to be partitioned more towards the intermetallic laves phase while Ni, Cr and Fe towards the gamma solid solution phase. The partitioning of Mo and Si towards the intermetallic phase and Ni toward the solid solution phase was more significant, whereas the partitioning of Fe and Cr in both the phases were found to be marginal (shown in figure 6). It was also observed that the dilution of Fe is more (of the order of 25–30%) near the substrate/clad interface and decreases down to 15% towards the surface of the clad. Thus the microstructure of the interfacial region exhibited a hypoeutectic structure (figure 4a) with coarser primary dendrites of proeutectic gamma solid solution with interdendritic lamellar eutectic (gamma + Laves). Some fine regions of Laves phase with globular morphology (∼200–300 nm) were also observed near the interface region. Proceeding towards the surface of the clad, the microstructure consisted of a near-eutectic structure of fine lamellar eutectic of gamma +

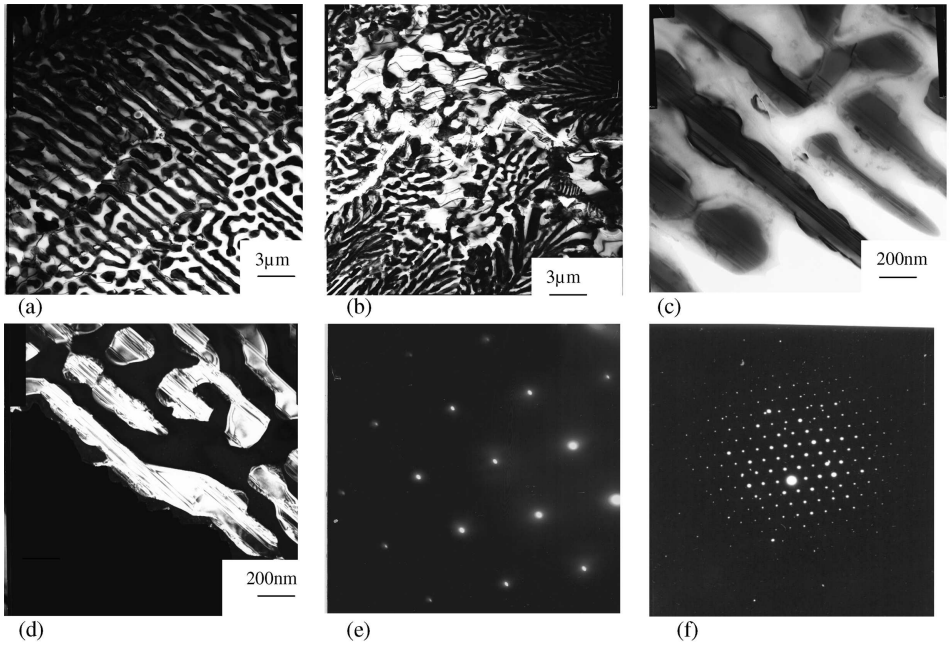

Figure 5. TEM micrographs showing (**a**), (**b**), (**c**) bright field images of the lamellar eutectic region, (**d**) dark field image, (**e**) SAED patterns in [0 1 1] zone axis of the fcc solid solution and (**f**) SAED pattern of the hcp intermatallic phase.

Laves phase (figure 4c). The nonhomogeneous structure is due to the fluctuation in the thermal field, convection fluid flow and associated instabilities, i.e. the motion of solid–liquid interface. At the interface, the solidification starts with planar front growth, because at the interface, compositional supercooling has least value as the substrate at the interface acts as heat sink, leading to high temperature gradient at liquid–solid interface and low solidification velocity. At very high G/R ratio planar solidification is obtained [6,7]. As the liquid–solid interface grows, the temperature gradient gradually decreases and solidification rate and compositional supercooling increases leading to change in the mode of solidification to cellular and dendritic. At the interface, the orientation of cellular dendrite is perpendicular to the substrate-clad interface as the substrate acts as a heat sink. Away from the interface, the orientation of cellular dendrite is related to local solidification direction which changes continuously towards the centre of the melt pool due to shift in the direction of the maximum thermal gradient. The interdendritic eutectic zone near interface region may be due preferential Mo segregation in the liquid phase because of lower solubility of Mo in Fe than in Ni. The rounded cellular morphology beyond interface may be due to reduced cooling rate because of substrate heating effect. The increase in iron dilution near the substrate/clad interface in the laser clad layer resulted in decrease in volume fraction of primary Laves phase and change in microstructural feature to hypoeutectic (primary phase is gamma solid solution). The decrease in proportion of the Laves phase may be due to overall decrease in

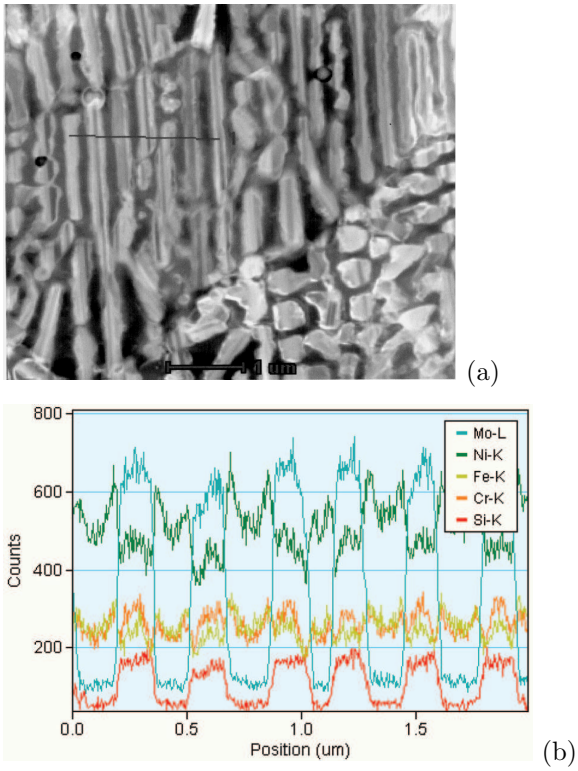

Figure 6. Composition variation (**b**) along the lamellar eutectic phases (**a**).

silicon content from original 3 wt% (as confirmed by EDS analysis), as silicon is known to increase the propensity for Laves phases in many systems [8].

4. Conclusion

Appropriate selection of laser cladding resulted in dense, defect-free and metallurgically bonded clad layers of Ni–Mo–Cr–Si alloy on stainless steel-316L substrate. Nonhomogeneous microstructure is due to the fluctuation in thermal field, convective fluid flow, and different rate of cooling and dilution from the substrate. The clad layers were characterized by the presence of hard molybdenum-rich hexagonal intermetallic Laves phase dispersed in relatively softer NiFe fcc gamma solid solution. Higher hardness in the clad is due to the fine structure and the presence of hard Mo-rich intermetallic Laves phase.

References

[1] K P Cooper, in *ASM handbook*, 10th ed. (ASM international, Metals Park, OH, 1992) Vol. 18, pp. 861–872

[2] C Williums, R C Crafer, P J Oakley (eds), *Laser processing in manufacturing* (Chapman and Hall, London, 1993) pp. 141–161
[3] W M Steen, *Laser materials processing* (Springer, London, 1991)
[4] C Navas, M Cadenas, J M Cuetos and J de Damborenea, *Wear* **260**, 838 (2006)
[5] R D Schmidt and D P Ferriss, *Wear* **32**, 279 (1975)
[6] W Kurz and D J Fisher, *Fundamentals of solidification* (Trans. Tech. Publication, Aedermansdorf, Switzerland, 1986)
[7] K A Jackson and J P Hunt, *Acta Metall.* **13**, 1212 (1965)
[8] R C Mittal, S K Si and K P Gupta, *J. Less Common Metals* **60**, 75 (1978)